Journal of Biomedical Optics 9(5), 1063–1073 (September/October 2004)

Three-dimensional optical tomographic brain imaging in small animals, part 2: Unilateral carotid occlusion

A. Y. Bluestone
Columbia University
Departments of Biomedical Engineering and Radiology
New York, New York 10027
and
State University of New York
Downstate Medical Center
Department of Pathology
Brooklyn, New York 11203

M. Stewart
State University of New York
Downstate Medical Center
Department of Physiology and Pharmacology
Brooklyn, New York 11203

B. Lei
I. S. Kass
State University of New York
Downstate Medical Center
Department of Physiology and Pharmacology
and
Department of Anesthesiology
Brooklyn, New York 11203

J. Lasker
G. S. Abdoulaev
A. H. Hielscher
Columbia University
Departments of Biomedical Engineering and Radiology
New York, New York 10027
E-mail: ahh2004@columbia.com

Abstract. This is the second part of a two-part study that explores the feasibility of 3-D, volumetric brain imaging in small animals by optical tomographic techniques. In part 1, we demonstrated the ability to visualize global hemodynamic changes in the rat head in response to elevated levels of CO_2 using a continuous-wave instrument and model-based iterative image reconstruction (MOBIIR) algorithm. Now we focus on lateralized, monohemispherically localized hemodynamic effects generated by unilateral common carotid artery (CCA) occlusion. This illustrates the capability of our optical tomographic system to localize and distinguish hemodynamic responses in different parts of the brain. Unilateral carotid occlusions are performed in ten rodents under two experimental conditions. In the first set of experiments the normal systemic blood pressure is lowered to 50 mmHg, and on unilateral carotid occlusion, we observe an ipsilateral monohemispheric global decrease in blood volume and oxygenation. This finding is consistent with the known physiologic response to cerebral ischemia. In a second set of experiments designed to observe the spatial-temporal dynamics of CCA occlusion at normotensive blood pressure, more complex phenomena are observed. We find three different types of responses, which can be categorized as compensation, overcompensation, and noncompensation. [DOI: 10.1117/1.1784472]

Keywords: optical tomography; brain imaging; carotid occlusion; small animal model; rodents.

Paper 03078 received Jun. 17, 2003; revised manuscript received Jan. 14, 2004; accepted for publication Jan. 26, 2004.

1 Introduction

In part 1, of this two part study, which explores the potential for 3-D small animal brain imaging, we described the model-based iterative image reconstruction (MOBIIR) algorithm as well as the dynamic optical imaging instrumentation employed to collect experimental measurement data. Furthermore, we provided a description of how we incorporate anatomical prior knowledge for the purpose of enhancing our spatial resolution, and gave an example of the image reconstruction's sensitivity to probe-versus-model positioning mismatch. We investigated the system's utility for *in-vivo* imaging by examining the global cerebrovascular responses to hypercapnia in rats. The work described in this second part was undertaken to evaluate the potential of our 3-D optical tomographic imaging system to detect and localize a focal monohemispheric perturbation. We report studies of the cerebrovascular responses to unilateral common carotid artery occlusion in rats.

Address all correspondence to Andreas H. Hielscher, Columbia University, Department of Biomedical Engineering, ET351 Mudd Bldg, MC8904, 500 West 120th St., New York, NY 10027, USA. Phone: 212 854 5080; Fax: 212 854 8725; E-mail: ahh2004@columbia.edu

Unilateral carotid artery occlusion was utilized because of this phenomenon's well-established physiology. In the rat, occlusion of a single common carotid artery causes only minor alterations in cerebral blood flow in the ipsilateral hemisphere.[1,2] These relatively minor alterations, nevertheless, even in the presence of an intact Circle of Willis, may produce transient lateralized hemodynamic changes. Furthermore, when a superimposed episode of systemic hypoxia or ischemia is present (e.g., by lowering of the blood pressure, thereby preventing effective collateral circulation, which manifests itself as systemic hypoxia), unilateral carotid artery occlusion is associated with ischemic neuronal injury in the ipsilateral hemisphere of the adult rat brain.[3] Therefore, we studied animals that had their mean systemic blood pressure lowered from about 100 to about 50 mmHg by direct withdrawal of blood, and then examined the changes induced in brains by clipping either common carotid artery (CCA), as a model for lateralized ischemic changes in the brain.

A second phenomenon that is well described in the literature is the postischemic reactive hyperemia that occurs following transient cerebral ischemia of varying durations.[4] Hy-

1083-3668/2004/$15.00

peremia is defined as cerebral blood flow (CBF) in excess of metabolic demands. When CBF is reduced, CBF and the metabolic rate of oxygen consumption ($CMRO_2$) often stay coupled, whereas in hyperemia, uncoupling of CBF and metabolism occurs. The temporal dynamics of reactive hyperemia have been studied experimentally[4,5] and have been simulated on computer.[6] It has been observed that reactive hyperemia is a function of the length of the ischemic interval: as one increases the interval, for a period of time less than that required for tissue necrosis to set in, the overshoot is linearly related to the length of the occlusive interval.[4]

The capability of near-infrared spectroscopy to detect and quantify the carotid-occlusion-induced change in cerebral oxygenation was shown previously by Fantini et al.[7] They observed that a unilateral interruption in the carotid blood flow of a piglet at physiologic blood pressure (100 mmHg) did not significantly affect cerebral oxygenation. Bilateral occlusion, however, caused a significant decrease in tissue perfusion. They also observed that after clip removal, an overshoot of cerebral oxygenation occurred followed by a return to baseline. These studies were performed using eight source fibers and a single detector fiber, and no spatial maps (2-D or 3-D) were generated.

Other relevant cerebrovascular occlusion studies in small animals, have been reported. For example, in an early work, Lodder's group reported on stroke-induced changes in the NIR spectrum of gerbil brains.[8,9] The authors obtained spectra in the wavelength range from $\lambda = 1400$ to 2400 nm from over 50 frozen and living gerbil brains, and attributed the observed spectral changes during ischemia (induced by closing the carotid arteries) to changes in protein and lipid composition. However, the long wavelengths used by Carney et al. do not permit light to penetrate deep into the brain, and all following work has been focused on shorter wavelengths between $\lambda = 600$ and 900 nm.

As already mentioned in part 1, Wolf et al. reported on optically measuring peri-infarct depolarization (PID) in focal cerebral ischemia in rats,[10] and concluded that NIRS is capable of noninvasive detection of a ''fingerprint'' of PID in rats. More recently, Chen et al.[11,12] performed optical studies using an intracranial infarction model in rats. They generated a topographic map of optical density changes between pre- and post-middle cerebral artery occlusion, and these showed good correlation with magnetic resonance images as well as histological stained slices of the same animal. 2-D topographic maps that show blood-volume dynamics were also generated by Fantini, Franceschini, and Gratton,[13] who monitored subcortical injection of autologous blood in piglet heads. These maps were generated by back-projecting the changes in the absorption coefficients along the straight-line paths between sources and detectors.[14]

The goal of our studies is to go beyond topographic maps and obtain 3-D, volumetric reconstructions of the hemispheric changes in optical properties inside a rat head. This second work is arranged as follows. First, we describe the animal preparation and experimental methods employed. Then we report on the system's utility *in-vivo* by examining the cerebrovascular hemodynamic response to unilateral carotid occlusion at normotensive and hypotensive blood pressure. Finally, we describe the postischemic reactive hyperemic temporal changes observed during intermittent carotid occlusion of varying duration.

2 Methods

2.1 *Animal Preparation and Experimental Protocol*

Ten male rats (5 Wistar, 5 Sprague-Dawley), weighing 300 to 325 gm were used in this study. During surgery the rats were placed in the supine position on a heating blanket. Both common carotid arteries (CCAs) were exposed through a ventral midline incision of the neck after dissection between the sternocleidomastoid and the sternohyoid muscles parallel to the trachea. Each CCA was freed from its adventitial sheath and vagus nerve, which was carefully separated and maintained. The rats were tracheotomized and mechanically ventilated. Body temperature was maintained at 37° by utilizing a heating lamp. A femoral artery catheter was placed to monitor blood pressure. The animals were then transferred and their heads fixed in the stereotaxic frame. To monitor the cortical hemodynamic changes, an optical probe was mounted on a stereotaxic manipulator and positioned between the bregma and lambda suture lines (part 1, Fig. 1). After a stabilization period of 15 min, a baseline scan using all 48 source-detector pairs was performed on the forehead overlying both hemispheres. Blood pressure data as well as optical data were saved online on a PC. Each scan took ~ 5 min.

In the five Wistar rats, sutures were placed loosely around the carotids, and vascular clips were used to occlude either of the vessels. Optical measurements were continuously recorded through the experiment. During the initial optical measurements, the blood pressure was lowered to ~ 50 mmHg by removing arterial blood from the femoral catheter. After a stable 1-min period of baseline activity at a reduced blood pressure of 50 mmHg, the left CCA was occluded for 30 to 90 seconds. After the rat's brain hemodynamic activity recovered back to baseline levels, the same procedure was performed on the right side. During this entire procedure, the head remained fixed in the stereotaxic frame, thereby securing the identical position of the scanning points for all the subsequent optical measurements performed on a given rat.

Furthermore, five Sprague-Dawley rats were used to study the changes induced in rat brains by occluding the right carotid artery at normotensive blood pressure as a potentially global perturbation to cerebral blood flow. A vascular occluder (model OC2, In Vivo Metric, Ukiah, California) was sutured around the right CCA and the skin was closed with stitches for carotid artery occlusion via an air-filled syringe. In these experiments the occlusion, at physiologic blood pressure, was performed for a fixed period of time: 30, 60, and 90 s.

All coronal sections presented in this section correspond to the slice located midway between the lambda and bregma suture lines and are denoted with an asterisk in Fig. 1 of part 1.

3 Results

3.1 *Carotid Occlusion under Hypotensive Blood Pressure*

Figure 1(a) (upper row) displays the rat's blood pressure, Fig. 1(b) (middle row) shows a simultaneous trace of a single

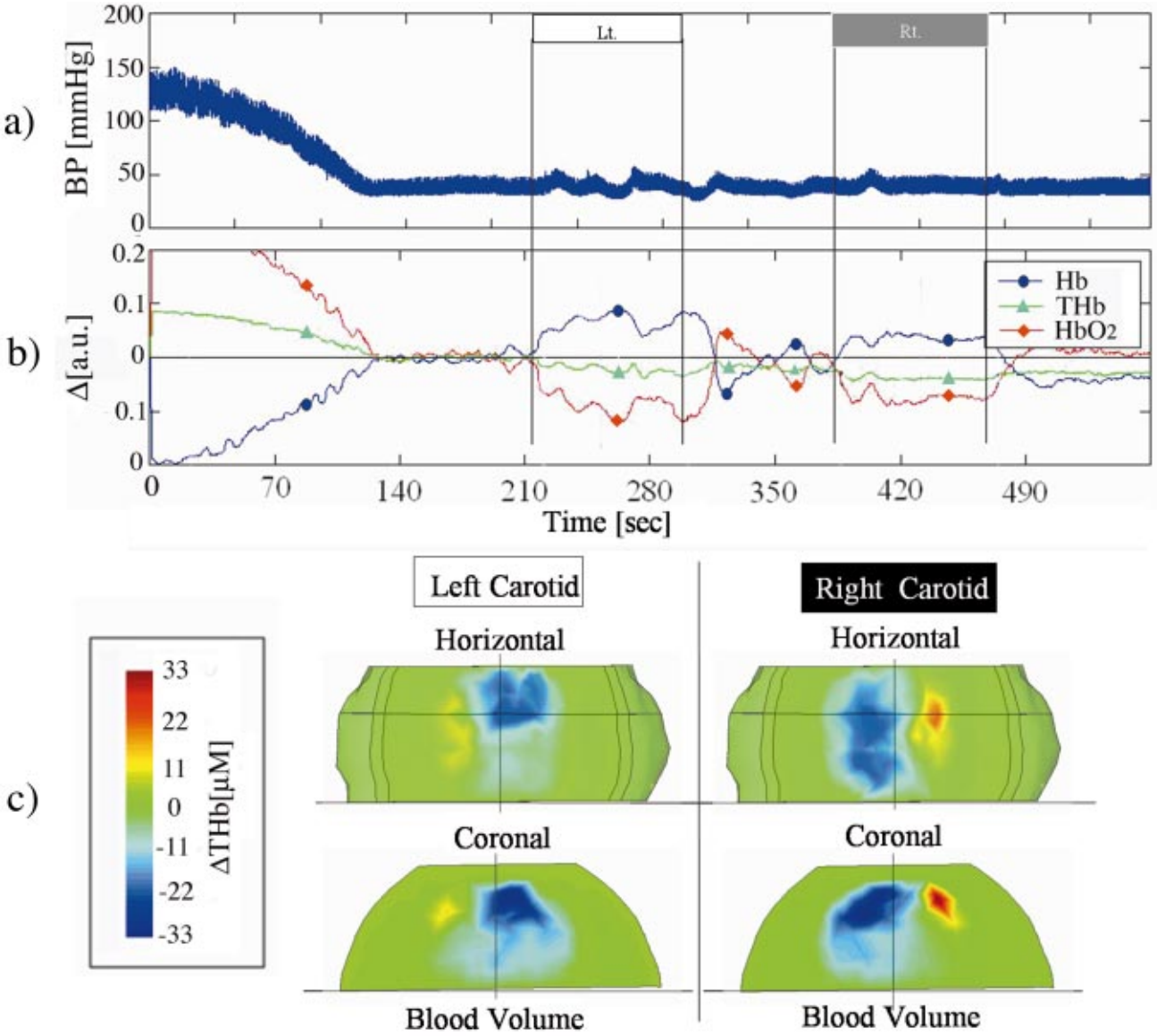

Fig. 1 Blood pressure changes and reconstructions of near-infrared signal intensity changes in the rat head during separate left and right carotid artery occlusions. (a) Continuous invasive blood pressure record. (b) Continuous optical signal intensity changes for source one (S1) and detector twelve (D12; see Fig. 2, part 1) during left carotid (horizontal white bar) followed by right carotid (horizontal gray bar) artery occlusion at a mean arterial blood pressure of approximately 50 mmHg. The blood pressure was lowered to this level prior to carotid occlusion by the withdrawal of whole blood (see Methods in Sec 2). (c) Representative horizontal and coronal image reconstructions midway during the periods of left and right carotid artery occlusion, respectively. Horizontal views were taken 2 mm below the upper surface of the rat's head. Coronal sections were midway between bregma and lambda. These figures demonstrate the volumetric imaging capabilities of our MOBIIR algorithm.

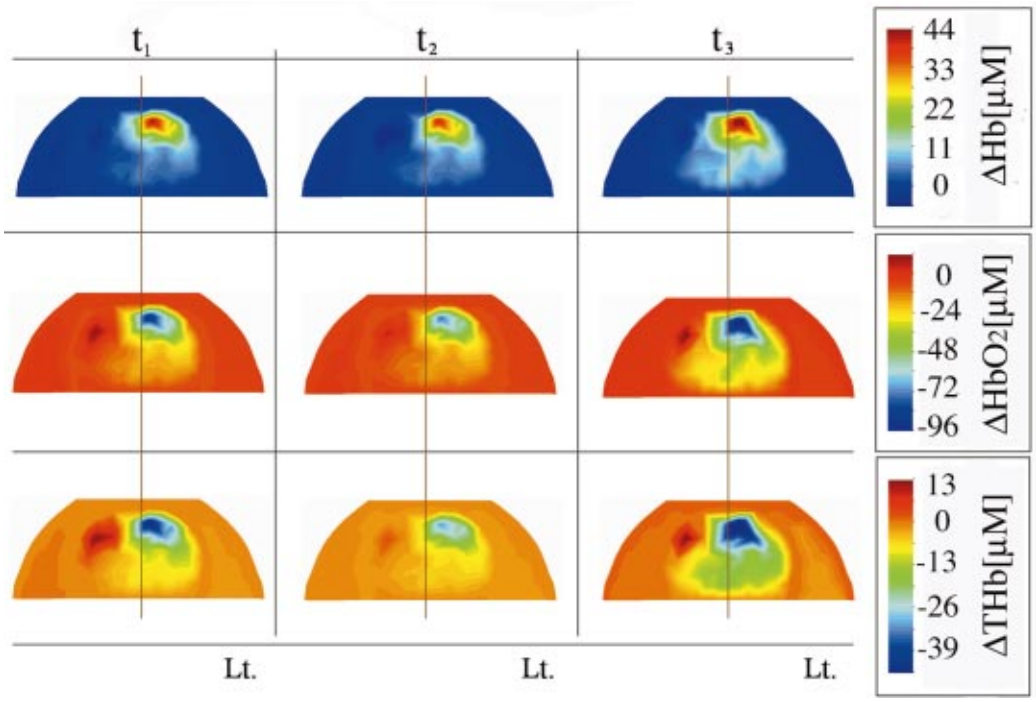

Fig. 2 Lateralized changes in hemoglobin concentrations during transient left carotid artery occlusion. Reconstructed images displaying coronal sections of the rat head show a lateralized increase in deoxyhemoglobin (Hb) and a decrease in oxyhemoglobin (HbO_2) and total hemoglobin (THb) on the side ipsilateral with the left carotid occlusion. The three time points ($t_{1,2,3}$=245 s, 255 s, 265 s; all during the period of occlusion) show very similar spatial hemodynamics to each other, and the decrease in oxyhemoglobin is approximately twice as large as the increase in deoxyhemoglobin.

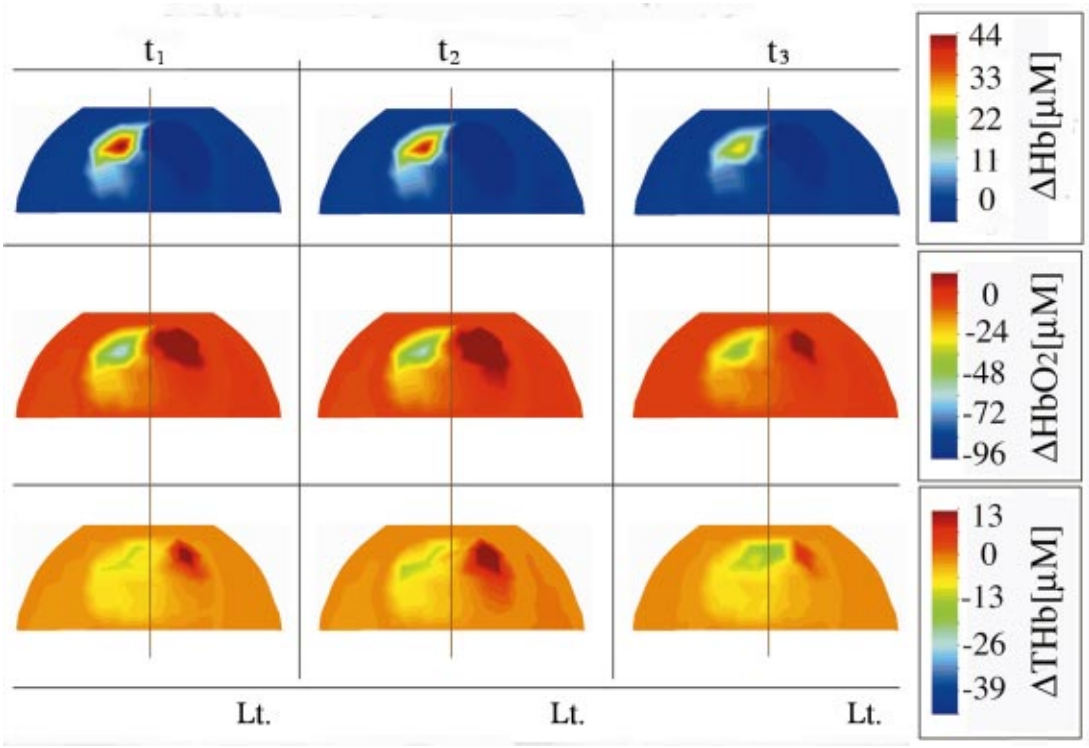

Fig. 3 Reconstructed images displaying coronal sections of the rat head showing a lateralized increase in deoxyhemoglobin and a decrease in oxyhemoglobin and total hemoglobin on the side ipsilateral with the right carotid occlusion. The three time points ($t_{1,2,3}$=420 s, 430 s, 440 s; all during the period of occlusion) show very similar hemodynamics to each other, and the decrease in oxyhemoglobin is approximately twice as large as the increase in deoxyhemoglobin. Note also the similarities in spatial extent of changes in hemoglobin to those shown for left carotid occlusion (Fig. 2).

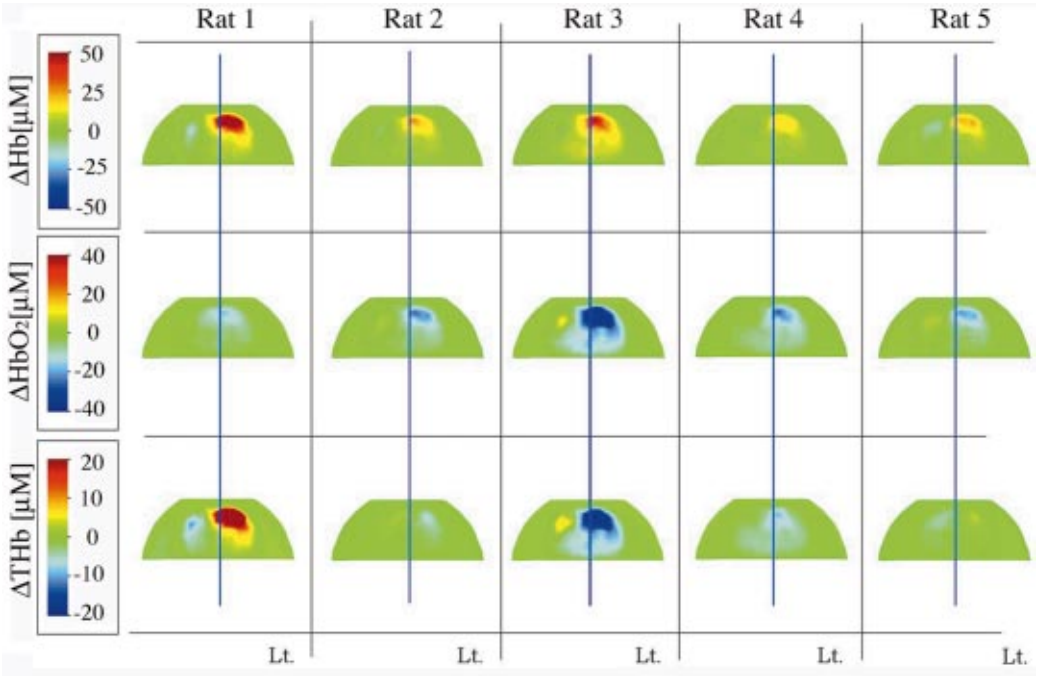

Fig. 4 Comparison of hemodynamic changes in a set of five rats during transient left carotid artery occlusion. Hemodynamic response are shown in coronal sections at a blood pressure of 50 mmHg. In four out of five rats, an ipsilateral decrease in oxyhemoglobin and blood volume can be observed. Note that the direction of change is consistent between rats, except for the lower total hemoglobin image for rat 1. The largest variations are seen in the total hemoglobin maps.

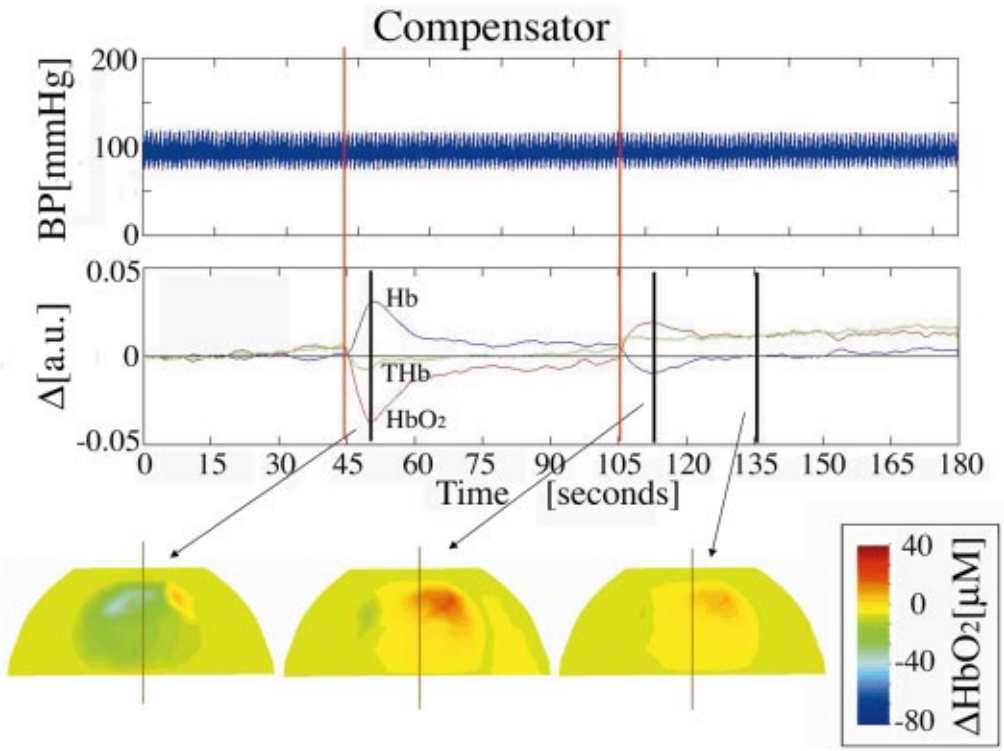

Fig. 5 The compensatory response to transient right carotid artery occlusion. An initial increase in deoxyhemoglobin and decrease in oxyhemoglobin are restored to near initial conditions during the period of carotid artery occlusion (first vertical red line marks the start of occlusion). A transient increase in oxyhemoglobin and decrease in deoxyhemoglobin are caused by the restoration of carotid arterial blood flow (second vertical red line). The top trace shows the stability of the blood pressure during the experiment. Middle trace shows a signal change for S1 to D12. The onset of right carotid occlusion (first red line, $t=45$ s) leads to an initial decrease in blood oxygenation on the side of the occlusion (left image), followed by a strong compensatory increase in oxygenation on the left side (middle image), and then it approaches baseline.

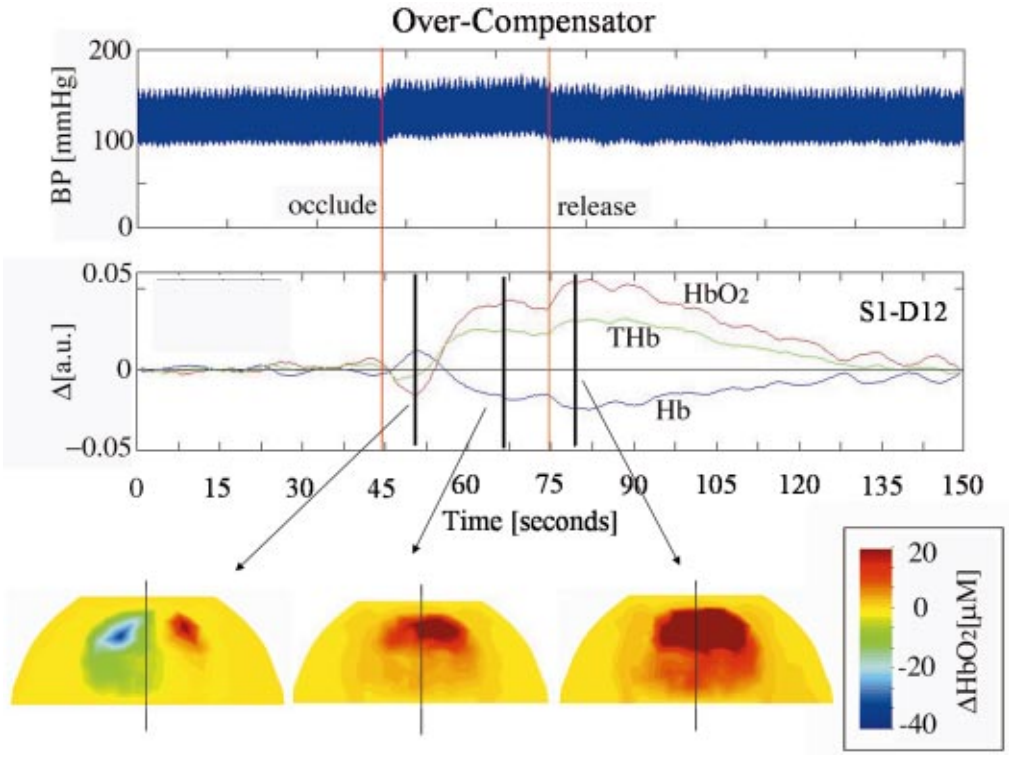

Fig. 6 The overcompensatory response to transient right carotid artery occlusion. An initial increase in deoxyhemoglobin and decrease in oxyhemoglobin were followed by a pronounced increase in oxyhemoglobin and decrease in deoxyhemoglobin during the period of carotid artery occlusion (vertical red lines mark the onset and offset of occlusion). The increase in oxyhemoglobin and decrease in deoxyhemoglobin persisted for nearly a minute after carotid blood flow was restored. The top trace shows an increase in blood pressure during the occlusion. Middle trace shows signal change for S1 to D12. The right carotid occlusion (red line at $t=45$ s) leads to an initial decrease in blood oxygenation on the side of the occlusion (left image), followed by an overcompensatory increase on the left prior to release of the vascular clip (middle image, $t=67$ s), and finally a strong compensatory increase in oxygenation on both sides (right image, $t=80$ s) after release of the clip. Note the initial increase in oxygenation occurs before release of the cuff (second red line at $t=75$ s).

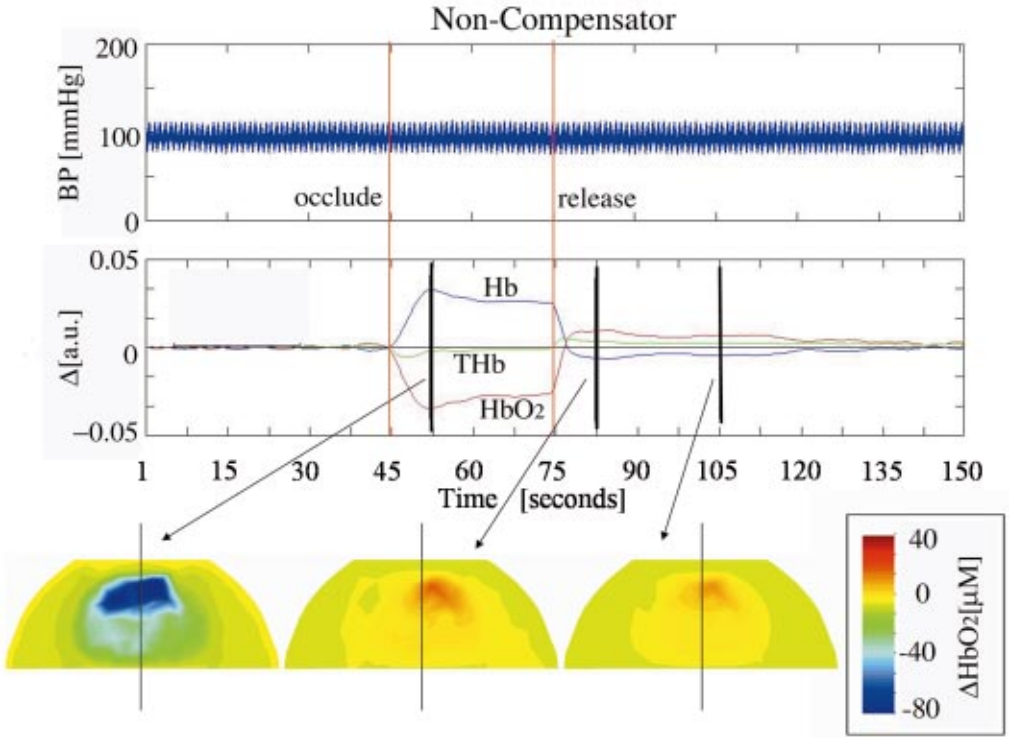

Fig. 7 The noncompensatory response to transient right carotid artery occlusion. The initial increase in deoxyhemoglobin and decrease in oxyhemoglobin persisted for the entire period of arterial occlusion and showed modest reversals only after carotid blood flow was restored. The top trace shows the stability of blood pressure during the experiment. The middle trace shows signal change for S1 to D12. The right carotid occlusion (red line at $t=45$ s) leads to a decrease in blood oxygenation on the side of the occlusion (left image). This is maintained for the extent of the occlusion and upon release (second red line at $t=75$ s) is followed by a strong compensatory increase in oxygenation on both sides (middle image), which slowly returns to baseline (right image).

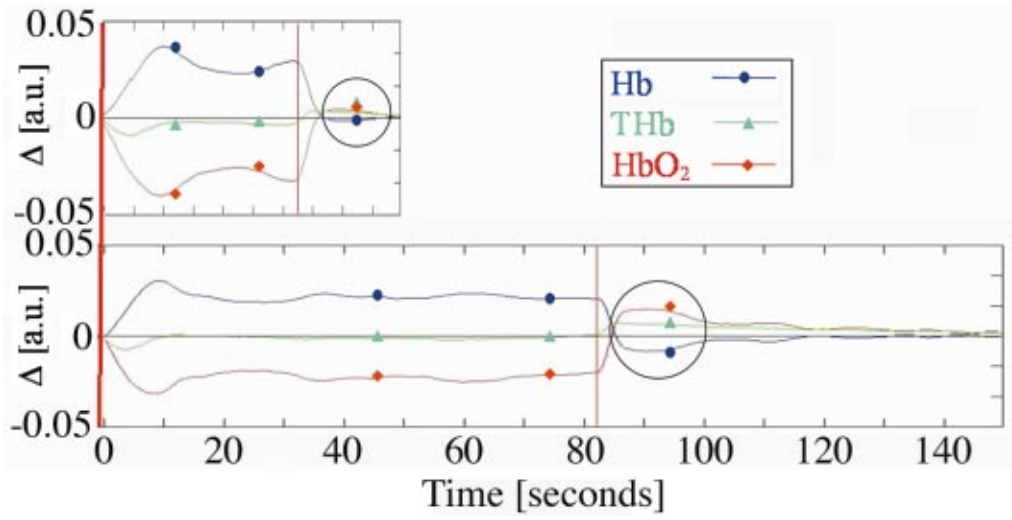

Fig. 8 Properties of reactive hyperemic responses for two different durations of carotid occlusion. Top trace: carotid occlusion was maintained for 30 s. Bottom trace: carotid occlusion was maintained for 80 s. One can observe that the duration of reactive hyperemia is larger when the occlusion is maintained for a longer period of time.

source-detector pair (S1 through D12), and in Fig. 1(c) (bottom row) one can see two views of the reconstructed 3-D volumes during left and right carotid occlusion. Since we were interested in determining the relative change in hemoglobin caused only by carotid occlusion and not the change caused by the lowering of blood pressure, the optical trace was normalized once the blood pressure had stabilized. In Fig. 1(a), the initial decrement of blood pressure to a mean arterial pressure between 40 and 50 mmHg can be seen. In Fig. 1(b), the normalized optical trace corresponding to the plateau period between time points 120 and 210 s is shown. After a stabilization time of ~60 s, the left carotid artery (white bar, $t=210$ to 300 s) was occluded with a vascular clip. After the occlusion, one can clearly see an increase in deoxyhemoglobin (Hb) and a drop in both oxyhemoglobin (HbO_2) and total hemoglobin (THb). On release of the clip at $t=305$ s, we observed an initial hyperemic overshoot followed by a gradual oscillatory return to baseline (other source-detector channels showed fewer oscillations). At $t=385$ s, the right common carotid artery was occluded (gray bar, $t=385$ to 470 s) and once again a decrease of deoxyhemoglobin was observed, but the change in signal was smaller than that observed by the left occlusion. This observation is reasonable because the source-detector pair displayed [Fig. 1(b)] was located predominantly on the left side of the rat's head. Note, just as in part 1, the singe source-detector trace was used to generate an easily visualized plot of the change in hemoglobin oxygenation as a function of time. Individual trend plots of a single source-detector pair were used only to select times of interest, and at those time points, full tomographic (all 48 source-detector combinations) image reconstructions were performed. It is only after performing an image reconstruction that we report concentration changes in total hemoglobin, as depicted in the horizontal and coronal sections in Fig. 1(c). These images were generated using all source-detector information at $t=250$ s, and $t=410$ s, respectively. The lateralization of the response can be clearly seen in both the horizontal and coronal views.

To gauge the variability of the resulting volumetric hemodynamic change, time points evenly spaced within the middle of each perturbation (left versus right) were selected. At each of these time points a full tomographic reconstruction was performed. Three time points were selected for display and are depicted in Figs. 2 and 3. In Fig. 2, one can observe the resulting reconstructions for a coronal slice taken midway between the bregma and lambda suture lines. The lateralization of the response can be clearly seen. The ipsilateral side shows an increase in deoxyhemoglobin and a decrease in both oxyhemoglobin and blood volume. A mirror image response was observed on right carotid artery occlusion (Fig. 3). However, the contralateral (nonoccluded) side showed a stronger increase in oxyhemoglobin and total hemoglobin than the contralateral side seen with left carotid occlusion.

In Fig. 4, the vascular response to left carotid occlusion across five rats is shown. The upper row displays the change in deoxyhemoglobin, the middle row the change in oxyhemoglobin, and the bottom row the change in total hemoglobin, defined as the sum of oxyhemoglobin and deoxyhemoglobin. In all five rats (five columns), one can observe an ipsilateral decrease in oxyhemoglobin and an increase in deoxyhemoglobin during left carotid occlusion at a blood pressure of 50 mmHg. This figure demonstrates the reproducibility of the location of the effect, and quantifies these changes by using a fixed color scale for each hemoglobin parameter across all animals. Qualitatively, one can observe that the direction of change is reproducible for all oxyhemoglobin and deoxyhemoglobin maps, and that the magnitude of these changes is within a factor of 2 of each other; except for one outlier (rat 1) that shows an increase in total hemoglobin.

3.2 *Carotid Occlusion under Normotensive Blood Pressures*

After being satisfied that monohemispheric responses could be imaged, we explored the possibility of studying more complex responses at normotensive blood pressures in another five rats. Performing the right carotid occlusion experiments at physiologic blood pressure, we observed three different types of responses. In Figs. 5, 6, and 7, one can observe the change in hemoglobin species for a single source-detector pair as well as the corresponding image reconstructions at the marked points. Two of the rats showed a compensatory response (Fig. 5), where right carotid occlusion (first red line, $t=45$ s) leads to an initial decrease in oxygemoglobin on the side of the occlusion (left image, $t=50$ s). This gradually tapers to baseline (right image, $t=135$ s). On release of the vascular occluder ($t=105$ s), a hyperemic overshoot is observed (middle image $t=112$). Note that during the extent of the occlusion, the blood pressure remains relatively constant (compare with Fig. 6).

Two other rats showed an overcompensatory type of response, as depicted in Fig. 6. The occlusion (first red line, $t=45$ s) leads to an initial decrease in oxyhemoglobin on the ipsilateral side, followed by a relatively large overshoot in oxyhemoglobin and blood volume. This overshoot occurs even before releasing the vascular occluder (middle image, $t=67$ s). On release (second red line, $t=75$ s), a further increase in blood oxygenation occurs. Note that during the perturbation ($t=45$ to 75), a mean increase in blood pressure of 10 mmHg was observed. The coronal sections, at the selected time points, seem to indicate that while the initial occlusion only decreases oxyhemoglobin on the ipsilateral side (left image, $t=50$ s), the overcompensation increases oxyhemoglobin in both hemispheres. This increase is asymmetric with the contralateral side showing a larger increase. On release of the vascular clip, a more global (symmetric) increase in oxygenation is observed in both hemispheres (right image, $t=80$ s).

One experiment revealed a noncompensatory type of response (Fig. 7), where the right carotid occlusion (first red line, $t=45$ s) leads to a decrease in blood oxygenation on the side of the occlusion (left image). This decrease is maintained for the extent of the occlusion and then, upon release (second red line, $t=75$ s) of the vascular occluder, a strong compensatory increase in oxygenation on both sides (middle image, $t=82$ s) is observed. This increase slowly returns to baseline (right image, $t=105$ s).

3.3 *Reactive Hyperemia*

For the noncompensating rat, we compared the magnitude of the reactive hyperemia after maintaining the carotid occlusion for two different time intervals. In the upper trace in Fig. 8, the right carotid occlusion was maintained for ~30 s, and in

the lower trace it was maintained for ~80 s. One can observe that the hyperemic overshoot (black circles) and extent of the reactive hyperemia is proportionally greater when the occlusion is maintained for a longer period of time.

4 Discussion

4.1 *Carotid Occlusion under Hypotensive Blood Pressure*

With the onset of the occlusion, the ipsilateral side demonstrated a drop not only in oxyhemoglobin but also in total hemoglobin in four out of five rats. Experimentally, we observed decreases of 20–40 μM in the total hemoglobin concentration when either left or right common carotid artery occlusion was induced at a reduced blood pressure of 50 mmHg, except in a single outlier. A concurrent increase in deoxyhemoglobin of 30–50 μM was observed as well. The decrease in cerebral total hemoglobin was found to be present over the ipsilateral cortex, and appears to be constrained with respect to the midsagittal plane. Across five rats the spatial localization of the ischemic area was similar with unilateral CCA occlusion, and the relative maximum decrease in oxyhemoglobin and increase in deoxyhemoglobin in the ipsilateral hemisphere had a mean and standard deviation of -20 ± 7 μM, 30 ± 10 μM, respectively. Since we normalize each experiment to its own baseline during the initial measurement period, the overall change is a function of the animal's baseline condition, similar to our findings during the hypercapnia studies (see part 1). The reason for the outlier is not clear at this time, but could have been caused, for example, by inaccurate probe placement.

4.2 *Carotid Occlusion under Normotensive Blood Pressure*

As mentioned in the introduction, considerable difference can be expected with respect to the hemodynamic responses to carotid occlusion under normotensive and hypotensive blood pressure. The autoregulatory mechanisms of the cerebrovasculature are very much intact when the experiment is performed at normotensive blood pressure, and therefore one would expect to observe only transient changes in the local cerebral hemodynamics. Hence, in the set of right CCA occlusion experiments performed at normotensive blood pressure, we paid particular attention to the temporal dynamics of the event. While Fantini et al.,[7] performing optical studies, reported on one type of hemodynamic response, we observed three different types of reactions, which we defined as compensation, overcompensation, and noncompensation.

The first type of response, compensation, was what we initially expected to observe based on the work described by Fantini et al.[7] One sees an initial decrease in blood oxygenation on the side of the occlusion, and a small compensatory increase in oxygenation on the contralateral side (Fig. 5, $t = 50$ s). The increase in oxygenation gradually tapers and approaches but does not quite reach the baseline that was present before the occlusion. After release of the carotid occluder, a strong compensatory increase contralateral to the occlusion is observed. Interestingly, in this case no change in blood pressure (BP) was observed (Fig. 5, top row).

In the second type of response, overcompensation, the occlusion led to an initial decrease in oxyhemoglobin on the ipsilateral side, as was seen in the compensation-type of response. This initial decrease was followed by a relatively large overshoot in oxyhemoglobin and total hemoglobin. This response occurred within a few seconds of occlusion. We believe that a large part of this overshoot is attributable to the sudden increase in blood pressure observed in the BP trace (Fig. 6, top row). However, a portion of the signal change cannot be attributed to blood pressure, because on releasing the vascular occluder, even though blood pressure returned to baseline immediately, the optical signal continued to increase, and required ~60 s to recover (Fig. 6). The displayed coronal sections showed that this compensatory increase crossed over the midline to the contralateral side, oversupplying both the nonoccluded and occluded hemisphere.

In the third type of response displayed in Fig. 7, noncompensation, the right carotid occlusion led to a decrease in blood oxygenation on the side of the occlusion. This decrease remains for the extent of the occlusion; evidently, the animal is unable to correct the hypoperfusion of the affected hemisphere. Upon release of the vascular occluder, a slight compensatory increase in oxygenation is observed. In this animal, the lack of a compensatory response to carotid occlusion is mysterious. It is possible that the occlusion itself caused neural damage that prevented a compensatory response. Alternatively, some animals may be minimally responsive and therefore constitute a group of animals that would be especially vulnerable to carotid occlusion.

4.3 *Reactive Hyperemia*

In all three types of responses, a reactive hyperemia was observed on release of the vascular occluder (see Figs. 5, 6, and 7), as reported previously in the literature. For example, reactive hyperemia has been measured optically by Mayevsky et al.[5] In their work, a multifunctional tissue spectroscopic probe was used to simultaneously monitor the microcirculatory blood flow, tissue reflectance, and the intramitochondrial NADH redox state of the rat brain. The probe was inserted into the parietal lobe of the rat brain, and data were collected during the occlusion and immediately following the release, which occurred after 10 s. They observed a postischemic hyperemic increase in total blood flow as well as total blood volume. The blood flow change was measured using laser Doppler flowmetry, while the blood volume change was measured using optical reflectance spectroscopy.

Furthermore, Gourley and Heistad[15] have described that reactive hyperemia is a function of the length of the ischemic interval; as one increases the interval, for a period of time less than that required for tissue necrosis to set in, the overshoot (duration of reactive hyperemia) is proportionally related to the length of the occlusive interval. This was determined using cats, in which ischemia was produced with an inflatable pediatric cuff wrapped around the animals' neck. To maintain constant mean arterial blood pressure during reactive hyperemia, the distal abdominal aorta was cannulated and connected to a reservoir system. CBF was measured with microspheres during a control state, and after intervals of 5, 15, 60, and 300 s. We investigated the quantitative increase after occluder release as a function of the temporal extent of occlusion in the noncompensating type of rat (Fig. 8). The noncom-

pensating type of rat was selected because the extent of the occlusion did not significantly alter the hemodynamics during the occlusive period. This criterion was necessary, as we had no other means of maintaining a constant mean arterial blood pressure. The observed response appears to show the general trend described in the literature; that as the length of occlusion is increased the duration of reactive hyperemia is proportionally greater as well.[15]

It is worthwhile mentioning that we found that by using a vascular occluder, a greater level of reproducibility of the experimental protocol is achievable (less human error in location of occlusion). Furthermore, there is less resulting motion (not necessary to pull on suture), and the temporal interval of the occlusion can be more precisely controlled.

4.4 *Spatial Variability*

In comparing the results of part 2 of this study with those of part 1, one can note by visual inspection of the coronal sections that less variability is present between equally spaced time points during carotid occlusion than during hypercapnia. This observation is consistent with the known dynamics of hypercapnia, where moment-to-moment regulations of CBF are expected. By contrast, in our studies of unilateral carotid occlusion, the ipsilateral side is affected more aggressively, and that side is incapable of adjusting to the ischemic state. The contralateral side, however, does display a greater degree of hemodynamic variability.

5 Conclusion

The experiments in this two-part study were designed to explore the ability of 3-D optical tomography to capture spatial and temporal hemodynamic effects in the brains of small animals. In part 1, we described the instrumentation and model-based iterative image reconstruction algorithm that were used in all subsequent experiments. We first used the optical tomographic imaging system to investigate the global cerebral hemodynamic effects induced by increasing the concentration of inspired CO_2. As expected, we observed a linear relationship between the inhaled CO_2 concentration and the levels of oxyhemoglobin and blood volume in the rat brain. We were able to image and visualize the global progression of this effect.

In part 2, we reported on experiments involving unilateral carotid occlusion at normal and hypotensive blood pressure values. These studies allowed us to evaluate the ability of our tomographic imaging system to localize spatially dependent hemispheric hemodynamic events. The results of experiments at reduced blood pressure (50 mmHg) showed an average ipsilateral decrease of approximately 20–40 μM in total hemoglobin concentration when either left or right common carotid artery occlusion is induced. A concurrent increase on the ipsilateral side in deoxyhemoglobin of 30–50 μM was observed as well. The decrease in cerebral total hemoglobin is found to be present over the ipsilateral cortex, and appeared to be constrained with respect to the midsagittal plane. The results obtained here for a model of cerebral vasoreactivity to carotid occlusion in a rat are in reasonable agreement with the data from the literature.

After establishing the feasibility of 3-D tomographic imaging with a well-known physiologic perturbation, we embarked on experiments that would allow us to visualize a less-established hemodynamic response. During unilateral carotid occlusion at normotensive blood pressure, we observe three types of hemodynamic responses, of which only one had been previously reported in the literature. In addition to the compensatory response, which is characterized by a transient ipsilateral decrease in oxyhemoglobin and blood volume which, within a few seconds, returns to baseline prior to release of the occluded CCA, we observed overcompensatory and non-compensatory responses. An overcompensatory reaction is characterized by a transient ipsilateral decrease in oxyhemoglobin and blood volume, followed by a sharp rise in oxyhemoglobin and blood volume in both hemispheres. In the non-compensatory case, the ipsilateral side demonstrates a drop in oxyhemoglobin and blood volume, but remains stable throughout the occlusive period. This response mimics the occlusion seen in hypotensive animals. Therefore, we suspect that in this case the animal was in distress.

Although these studies demonstrate the potentials of optical tomography for small animal imaging, further improvements can be envisioned. For example, using a larger number of sources and detectors that not only record backscattered light intensities, but also provide transmission data, may yield better spatial resolutions. Employing more than two wavelengths will most likely lead to improved accuracy in the determination of the oxyhemoglobin and deoxyhemoglobin concentration. In addition, a larger number of wavelengths will also provide access to other important physiological chromophores, such as cytochrome oxidase, and allow us to explicitly account for the contribution of water and lipids to the optical signal. Coupling optical measurement techniques with high-resolution imaging modalities such as computerized tomography (CT) or magnetic resonance imaging (MRI), could potentially provide more accurate anatomical information, which could be used to further enhance the spatial localization of physiological parameters that are only accessible optically, such as oxyhemoglobin and blood volume.

The next step in terms of small animal studies is to look at even more focal phenomena, which provide smaller signals and are therefore even harder to image. Examples of these types of studies would include middle cerebral artery occlusions, which are typically performed to model strokes in animal paw or whisker stimulations, which are used in functional brain imaging. In the future, these small-signal experiments will further elucidate the potential and limits of optical tomographic imaging techniques in small animals.

Acknowledgments

This work was supported in part by the National Institute for Biomedical Imaging and Bioengineering (NIBIB-R01-001900[Hidscher]), and the National Institute of Neurological Disorders and Stroke NINDS-R21-NS045160[Stewart], both part of the National Institutes of Health (NIH), the City of New York Council Speaker's Fund for Biomedical Research: Toward the Science of Patient Care and the Dean's Office of the College of Medicine at the State University of New York (SUNY) Downstate Medical Center in Brooklyn, New York.

References

1. P. Coyle and M. J. Panzenbeck, "Collateral development after carotid artery occlusion in Fischer 344 rats," *Stroke* **21**, 316–321 (1990).

2. G. De Ley, J. B. Nshimyumuremyi, and I. Leusen, ''Hemispheric blood flow in the rat after unilateral common carotid occlusion: evolution with time,'' *Stroke* **16**, 69–73 (1985).
3. S. Levine, ''Anoxic-ischemic encephalopathy in rats,'' *Am. J. Pathol.* **36**, 1–17 (1960).
4. J. K. Gourley and D. D. Heistad, ''Characteristics of reactive hyperemia in the cerebral circulation,'' *Am. J. Physol.* **246**, H52–H58 (1984).
5. A. Mayevsky, T. Manor, E. Pevzner, A. Deutsch, R. Etziony, and N. Dekel, ''Real-time optical monitoring of tissue vitality in vivo,'' *Proc. SPIE* **4616**, 30–39 (2002).
6. M. Ursino, ''A mathematical model of overall cerebral blood flow regulation in the rat,'' *IEEE Trans. Biomed. Eng.* **38**, 795–807 (1991).
7. S. Fantini, D. Hueber, M. A. Franceschini, E. Gratton, W. Rosenfeld, P. G. Stubblefield, D. Maulik, and M. R. Stankovic, ''Non-invasive optical monitoring of the new born piglet brain using continuous-wave and frequency-domain spectroscopy,'' *Phys. Med. Biol.* **44**, 1543–1563 (1999).
8. J. M. Carney, W. Landrum, L. Mayes, Y. Zou, and R. A. Lodder, ''Near-infrared spectrophotometric monitoring of stroke-related changes in the protein and lipid composition of whole gerbil brains,'' *Anal. Chem.* **65**, 1305–1313 (1993).
9. R. I. Dempsey, L. A. Cassis, D. G. Davis, and R. A. Lodder, ''Near-infrared imaging and spectroscopy in stroke research: Lipoprotein distribution and disease,'' *Ann. N.Y. Acad. Sci.* **820**, 149–169 (1997).
10. T. Wolf, U. Lindauer, U. Reuter, T. Back, A. Villringer, K. Einhäupl, and U. Dirnagl, ''Noninvasive near infrared spectroscopy monitoring of regional cerebral blood oxygenation changes during peri-infarct depolarization in focal cerebral ischemia in the rat,'' *J. Cereb. Blood Flow Metab.* **17**, 950–954 (1997).
11. W. G. Chen, P. C. Li, Q. M. Luo, S. Q. Zeng, and B. Hu, ''Hemodynamic assessment of ischemic stroke with near-infrared spectroscopy,'' *Space Med. Medical Eng.* **13**(2), 84–89 (2000).
12. C. Weiguo, G. Lu, and W. Lichty, ''Localizing the focus of ischemic stroke with near infrared spectroscopy,'' *Chin. Med. J. (Engl)* **115**(1), 84–88 (2002).
13. S. Fantini, M. A. Franceschini, and E. Gratton, ''Non-invasive optical mapping of the piglet brain in real time,'' *Opt. Express* **4**, 308–314 (1999).
14. M. Franceschini, V. Toronov, M. E. Filiaci, E. Gratton, and S. Fantini, ''On-line optical imaging of the human brain with 160-ms temporal resolution,'' *Opt. Express* **6**, 49–57 (2000).
15. J. K. Gourley and D. D. Heistad, ''Characteristics of reactive hyperemia in the cerebral circulation,'' *Am. J. Physiol.* **246**, H52–H58 (1984).